Title
A multiscale dynamo model driven by quasi-geostrophic convection

Authors
Calkins, Michael A
Julien, Keith
Tobias, Steven M
et al.

Publication Date
2015-10-10

DOI
10.1017/jfm.2015.464

Peer reviewed

J. Fluid Mech. (2015), *vol.* 780, *pp.* 143–166. © Cambridge University Press 2015
doi:10.1017/jfm.2015.464

A multiscale dynamo model driven by quasi-geostrophic convection

Michael A. Calkins[1,†], Keith Julien[1], Steven M. Tobias[2] and Jonathan M. Aurnou[3]

[1]Department of Applied Mathematics, University of Colorado, Boulder, CO 80309, USA

[2]Department of Applied Mathematics, University of Leeds, Leeds LS2 9JT, UK

[3]Department of Earth, Planetary and Space Sciences, University of California, Los Angeles, CA 90095, USA

(Received 12 February 2015; revised 3 July 2015; accepted 3 August 2015)

A convection-driven multiscale dynamo model is developed in the limit of low Rossby number for the plane layer geometry in which the gravity and rotation vectors are aligned. The small-scale fluctuating dynamics are described by a magnetically modified quasi-geostrophic equation set, and the large-scale mean dynamics are governed by a diagnostic thermal wind balance. The model utilizes three time scales that respectively characterize the convective time scale, the large-scale magnetic evolution time scale and the large-scale thermal evolution time scale. Distinct equations are derived for the cases of order one and low magnetic Prandtl number. It is shown that the low magnetic Prandtl number model is characterized by a magnetic to kinetic energy ratio that is asymptotically large, with ohmic dissipation dominating viscous dissipation on the large scale. For the order one magnetic Prandtl number model, the magnetic and kinetic energies are equipartitioned and both ohmic and viscous dissipation are weak on the large scales; large-scale ohmic dissipation occurs in thin magnetic boundary layers adjacent to the horizontal boundaries. For both magnetic Prandtl number cases the Elsasser number is small since the Lorentz force does not enter the leading order force balance. The new models can be considered fully nonlinear, generalized versions of the dynamo model originally developed by Childress & Soward (*Phys. Rev. Lett.*, vol. 29, 1972, pp. 837–839), and provide a new theoretical framework for understanding the dynamics of convection-driven dynamos in regimes that are only just becoming accessible to direct numerical simulations.

Key words: dynamo theory, geodynamo, geophysical and geological flows

1. Introduction

It is now generally accepted that many of the observed planetary and stellar magnetic fields are the result of convectively driven dynamos (Miesch 2005; Stanley & Glatzmaier 2010). Direct numerical simulations (DNS) of the complete set of governing equations are now routine practice, but remain limited to parameter values

† Email address for correspondence: michael.calkins@colorado.edu

that are quite distant from natural systems owing to the massive requirements for numerically resolving disparate spatiotemporal scales (e.g. Jones 2011). The stiff character of the governing equations, while an impediment to DNS, provides a possible path forward for simplifying, or reducing, the governing equations with the use of multiscale asymptotics (e.g. Julien & Knobloch 2007; Klein 2010). Balanced flows, in which two or more forces in the momentum equations are in balance, are particularly suitable for asymptotic analysis given the subdominance of inertial accelerations. Indeed, reduced models based on the geostrophic balance, in which the Coriolis and pressure gradient forces balance, have formed the backbone for theoretical and numerical investigations on the large-scale dynamics of the Earth's atmosphere and oceans for over 60 years (Charney 1948; Pedlosky 1987).

It is an unfortunate fact, however, that direct measurement of the forces present within the electrically conducting regions of natural systems are not possible. That most large-scale planetary and stellar magnetic fields are aligned with their respective rotation axes (e.g. Schubert & Soderlund 2011) suggests that the Coriolis force plays a key role in the magnetic field generation process, at least with respect to the large-scale dynamics. For the case of the Earth's liquid outer core, viscous stresses are likely to be small for large-scale motions there (Pozzo *et al.* 2013), and observations tracking the movement of the geomagnetic field show that typical convective time scales are significantly longer than the rotation period (Finlay & Amit 2011). These studies suggest that the large-scale dynamics within the core may be geostrophically balanced (Jault, Gire & Mouël 1988; Jackson, Bloxham & Gubbins 1993; Gillet *et al.* 2010; Schaeffer & Pais 2011; Gillet, Schaeffer & Jault 2012). Alternatively, it has been hypothesized that the Lorentz force can balance with the Coriolis and pressure gradient forces to yield magnetostrophically balanced motions at certain length scales within the core (Roberts 1988; Moffatt 2008). It can be argued that only geostrophically balanced dynamos have been observed with DNS (e.g. Soderlund, King & Aurnou 2012; King & Buffett 2013) (however, see the plane layer investigation of Rotvig & Jones (2002)).

In a seminal investigation, Childress & Soward (1972) demonstrated that laminar convection in a rotating plane layer geometry is capable of supporting dynamo action. They outlined three unique distinguished limits, or balances, in the governing equations that can occur based on the relative strength of the magnetic field, which they referred to as the weak field, intermediate field and strong field limits. Soward (1974) (denoted S74 hereafter) and Fautrelle & Childress (1982) (denoted FC82 hereafter) subsequently investigated the weak and intermediate field limits in greater detail; for both investigations the flows were weakly nonlinear. S74 showed that stable periodic dynamos exist in the weak field limit, whereas Fautrelle & Childress (1982) found that dynamos of intermediate field strength may be dynamically unstable and thus lead to strong field states as the flow saturates. For simplicity, we refer to both the S74 and FC82 cases as the Childress–Soward dynamo model (denoted by CSDM), since they were first discussed by Childress & Soward (1972) and the only difference between the two models is the strength of the magnetic field. The basis for the CSDM is that the Ekman number $Ek = \nu/2\Omega H^2$ is taken as a small parameter, where ν is the kinematic viscosity, Ω is the rotation rate and H is the depth of the fluid layer. In this case, convection is spatially anisotropic with large aspect ratio $H/\ell \gg 1$, where ℓ characterizes the small horizontal length scale of the convection (Chandrasekhar 1961). By expanding the flow variables in powers of $Ek^{1/6}$, a dynamical equation for the large-scale horizontal magnetic field is derived that is driven by the mean electromotive force (emf) generated by the small-scale

fluctuating velocity and magnetic fields. Because the CSDM utilizes a single time scale, it applies to order one thermal and magnetic Prandtl numbers, $Pr = \nu/\kappa$ and $Pm = \nu/\eta$, respectively, where κ is the thermal diffusivity and η is the magnetic diffusivity of the fluid.

The CSDM continues to provide an invaluable tool for understanding the differences between large-scale and small-scale dynamo action, as well as aiding the interpretation of results obtained from DNS studies. S74 showed that a dynamo driven by small-scale rapidly rotating convection is necessarily large-scale. Many of the key features predicted by S74, such as the vertical structure and oscillatory temporal evolution of the large-scale magnetic field, have been confirmed with low Ekman number DNS (e.g. Stellmach & Hansen 2004). Recent work has employed the CSDM for investigating kinematic dynamo action driven by rotating convection (Favier & Proctor 2013). Mizerski & Tobias (2013) have extended the CSDM to include the effects of fluid compressibility via the anelastic approximation, showing that density stratification tends to delay the onset of dynamo action and reduces the strength of the resulting magnetic field.

In the present work we develop a new multiscale dynamo model that possesses many similarities with the CSDM, but also significant differences. We refer to the new model as the quasi-geostrophic dynamo model, or QGDM. Like the CSDM, the small-scale, convective dynamics are geostrophically balanced to leading order, but remain time-dependent and fully nonlinear in the QGDM; our small-scale dynamical equations are a magnetically modified version of the quasi-geostrophic convection equations developed by Julien, Knobloch & Werne (1998) (see also Julien *et al.* (2006) for a generalized development). The strength of the magnetic field in the QGDM is asymptotically larger than that considered by FC82, but is not a strong field in the sense that the Lorentz force does not enter the leading order force balance. In addition to the small horizontal convective length scale ℓ, the QGDM includes large-scale horizontal modulations L_X that allow for a diagnostic thermal wind balance in the large-scale momentum equations. Coupled with the large-scale heat equation, the large-scale model (in the absence of a magnetic field) is the equivalent of the planetary geostrophic equations commonly employed in oceanography (Robinson & Stommel 1959; Welander 1959; Grooms, Julien & Fox-Kemper 2011) and atmospheric science (Phillips 1963; Dolaptchiev & Klein 2009) (the so-called β-effect has been neglected in the present work though it can easily be incorporated into the current model, e.g. see Grooms *et al.* (2011)). Because of the additional scale L_X, the QGDM also possesses a non-zero large-scale vertical magnetic field that is not present in the CSDM. Moreover, the new model utilizes three disparate time scales characterizing the small-scale convective dynamics, the large-scale magnetic evolution time scale and the large-scale thermal evolution time scale. Both low and order one magnetic Prandtl number cases are considered. The QGDM can be simulated numerically to gain insight into large-scale magnetic field generation in planets and stars, where we can utilize the success of previous non-magnetic work (e.g. Sprague *et al.* 2006; Julien *et al.* 2012*a*,*b*; Rubio *et al.* 2014; Stellmach *et al.* 2014), and the increases in computational power that have occurred since the work of CS72.

In § 2 we present the asymptotic development of the model. In § 3 we discuss some of the important features of the QGDM, its relationship with the CSDM, and possible applications to natural dynamos. Concluding remarks are given in § 4.

2. Model development

2.1. *Governing equations*

We consider a rotating plane layer geometry with rotation vector $\boldsymbol{\Omega} = \Omega\,\widehat{\boldsymbol{z}}$ and constant gravity vector $\boldsymbol{g} = -g\widehat{\boldsymbol{z}}$. The horizontal boundaries are located a vertical distance H apart with the layer heated from the bottom boundary and cooled at the top boundary. For simplicity, the fluid is assumed to be Newtonian and Boussinesq with density ρ and thermal expansion coefficient α. The governing equations are then non-dimensionalized utilizing the scales $\mathscr{U}$, ℓ, $\ell/\mathscr{U}$, ΔT, $\mathscr{P}$ and $\mathscr{B}$ for the velocity, length, time, temperature, pressure and magnetic field, respectively. In the rotating reference frame with coordinates (x, y, z) the dimensionless governing equations are then

$$\partial_t \boldsymbol{u} + \boldsymbol{u}\cdot\boldsymbol{\nabla}\boldsymbol{u} + \frac{1}{Ro}\widehat{\boldsymbol{z}}\times\boldsymbol{u} = -Eu\,\boldsymbol{\nabla}p + M\boldsymbol{B}\cdot\boldsymbol{\nabla}\boldsymbol{B} + \Gamma\,\theta\,\widehat{\boldsymbol{z}} + \frac{1}{Re}\nabla^2\boldsymbol{u}, \tag{2.1}$$

$$\partial_t\theta + \boldsymbol{\nabla}\cdot(\boldsymbol{u}\theta) = \frac{1}{Pe}\nabla^2\theta, \tag{2.2}$$

$$\partial_t\boldsymbol{B} = \boldsymbol{\nabla}\times(\boldsymbol{u}\times\boldsymbol{B}) + \frac{1}{Rm}\nabla^2\boldsymbol{B}, \tag{2.3}$$

$$\boldsymbol{\nabla}\cdot\boldsymbol{u} = 0, \quad \boldsymbol{\nabla}\cdot\boldsymbol{B} = 0, \tag{2.4}$$

where the velocity, pressure, temperature and magnetic field are denoted by $\boldsymbol{u} = (u,\ v,\ w)$, p, θ and $\boldsymbol{B} = (B^{(x)},\ B^{(y)},\ B^{(z)})$, respectively. Both the hydrostatic centrifugal force and magnetic pressure have been absorbed into the pressure gradient term $\boldsymbol{\nabla}p$. The dimensionless parameters are defined by

$$Ro = \frac{\mathscr{U}}{2\Omega\ell}, \quad \Gamma = \frac{g\alpha\Delta T\ell}{\mathscr{U}^2}, \quad Re = \frac{\mathscr{U}\ell}{\nu}, \quad Pe = \frac{\mathscr{U}\ell}{\kappa}, \quad Eu = \frac{\mathscr{P}}{\rho\,\mathscr{U}^2}, \tag{2.5a–e}$$

$$M = \frac{\mathscr{B}^2}{\rho\mu\,\mathscr{U}^2}, \quad Rm = \frac{\mathscr{U}\ell}{\eta}. \tag{2.6a,b}$$

Here, Ro is the Rossby number, Γ is the buoyancy number, Re is the Reynolds number, Pe is the Péclet number, Eu is the Euler number, M is the ratio of magnetic energy to kinetic energy, and Rm is the magnetic Reynolds number. The permeability of free space is denoted by μ. We recall that the thermal and magnetic Prandtl numbers characterizing the fluid properties are related to the above parameters via the relationships $Pe = RePr$ and $Rm = RePm$. Importantly, in the present work we denote dimensionless parameters that are based on the large-scale depth of the fluid layer with a subscript H, whereas parameters without this distinction utilize the small convective scale ℓ.

In what follows we assume that the horizontal bounding surfaces are impenetrable, stress-free and perfect thermal and electrical conductors such that

$$\partial_z u = \partial_z v = w = \partial_z B^{(x)} = \partial_z B^{(y)} = B^{(z)} = 0, \quad \text{at } z = 0, H/\ell, \tag{2.7}$$

$$\theta = \begin{cases} 1 & \text{at } z = 0, \\ 0 & \text{at } z = H/\ell. \end{cases} \tag{2.8}$$

The development given here parallels that of Julien & Knobloch (2007) and Grooms *et al.* (2011) for other multiscale models. We find that three disparate time scales

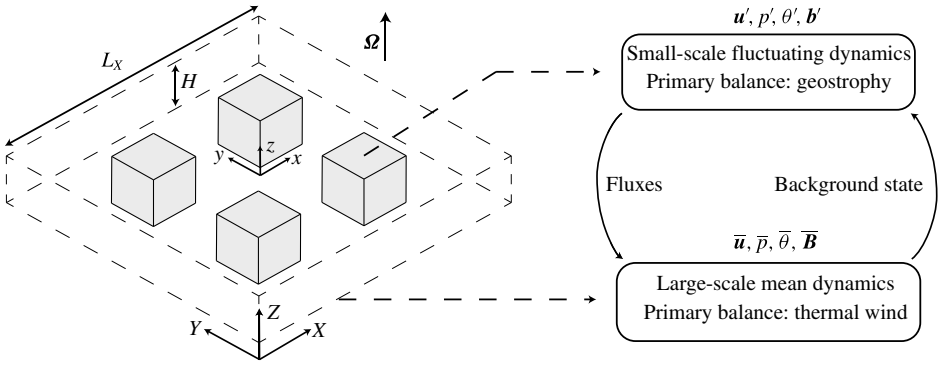

FIGURE 1. Schematic summarizing the general features of the multiscale dynamo model. The large-scale coordinate system is $\boldsymbol{X} = (X, Y, Z)$ and the small-scale coordinate system is $\boldsymbol{x} = (x, y, z)$; the shaded boxes depict small-scale subdomains embedded within the single large-scale domain. Large-scale mean dependent variables are given by $(\overline{\boldsymbol{u}}, \overline{p}, \overline{\theta}, \overline{\boldsymbol{B}})$ and the small-scale fluctuating dependent variables are $(\boldsymbol{u}', p', \theta', \boldsymbol{b}')$. Distinct equation sets are developed for the large-scale and small-scale domains, with the mean dynamics controlling the background state for the fluctuating dynamics and the fluctuating dynamics feeding back onto the mean state via small-scale fluxes.

are necessary to completely describe the temporal evolution of the dynamo; these are (1) the time scale of the small-scale convective fluctuations (denoted by t), (2) the large-scale magnetic evolution time scale (τ), and (3) the large-scale thermal evolution time scale (T). The small-scale, rapidly varying spatial and temporal coordinates are denoted as $(\boldsymbol{x}, t)$, and the slowly varying large-scale coordinates are given by $(\boldsymbol{X}, \tau, T)$. The fields are decomposed into mean and fluctuating components according to

$$\boldsymbol{u}(\boldsymbol{x}, \boldsymbol{X}, t, \tau, T) = \overline{\boldsymbol{u}}(\boldsymbol{X}, \tau, T) + \boldsymbol{u}'(\boldsymbol{x}, \boldsymbol{X}, t, \tau, T), \tag{2.9}$$

$$p(\boldsymbol{x}, \boldsymbol{X}, t, \tau, T) = \overline{p}(\boldsymbol{X}, \tau, T) + p'(\boldsymbol{x}, \boldsymbol{X}, t, \tau, T), \tag{2.10}$$

$$\theta(\boldsymbol{x}, \boldsymbol{X}, t, \tau, T) = \overline{\theta}(\boldsymbol{X}, \tau, T) + \theta'(\boldsymbol{x}, \boldsymbol{X}, t, \tau, T), \tag{2.11}$$

$$\boldsymbol{B}(\boldsymbol{x}, \boldsymbol{X}, t, \tau, T) = \overline{\boldsymbol{B}}(\boldsymbol{X}, \tau, T) + \boldsymbol{b}'(\boldsymbol{x}, \boldsymbol{X}, t, \tau, T), \tag{2.12}$$

and the fluctuating magnetic field vector is $\boldsymbol{b}' = (b'^{(x)}, b'^{(y)}, b'^{(z)})$. In figure 1 a schematic illustrating the general features of the model is shown. The mean quantities are defined as averages taken over the fast scales according to

$$\overline{f}(\boldsymbol{X}, \tau, T) = \lim_{t', \mathscr{V} \to \infty} \frac{1}{t' \mathscr{V}} \int_{t', \mathscr{V}} f(\boldsymbol{x}, \boldsymbol{X}, t, \tau, T)\, \mathrm{d}\boldsymbol{x}\, \mathrm{d}t, \quad \overline{f'} \equiv 0, \tag{2.13}$$

with the small-scale fluid volume denoted by $\mathscr{V}$. With multiple scales the differentials become

$$\partial_t \to \partial_t + \frac{1}{A_\tau}\partial_\tau + \frac{1}{A_T}\partial_T, \tag{2.14}$$

$$\boldsymbol{\nabla} \to \boldsymbol{\nabla} + \overline{\boldsymbol{\nabla}}, \tag{2.15}$$

where now $\boldsymbol{\nabla}$ only acts on the small-scale coordinates $\boldsymbol{x}$ and the large-scale, mean gradient operator is defined by

$$\overline{\boldsymbol{\nabla}} = \left(\frac{1}{A_X}\partial_X, \frac{1}{A_X}\partial_Y, \frac{1}{A_Z}\partial_Z \right). \tag{2.16}$$

The various aspect ratios are defined according to

$$A_X = A_Y = \frac{L_X}{\ell}, \quad A_Z = \frac{H}{\ell}, \quad A_\tau = \frac{t}{\tau}, \quad A_T = \frac{t}{T}. \tag{2.17a–d}$$

For simplicity we assume isotropic horizontal large-scale modulations (i.e. $A_X = A_Y$) in the present work, though the approach remains completely general.

The governing equations become

$$\left(\partial_t + \frac{1}{A_\tau}\partial_\tau + \frac{1}{A_T}\partial_T \right) \boldsymbol{u} + \boldsymbol{\nabla}\cdot\left(\boldsymbol{u}\boldsymbol{u}^{\mathrm{T}}\right) + \overline{\boldsymbol{\nabla}}\cdot\left(\boldsymbol{u}\boldsymbol{u}^{\mathrm{T}}\right) + \frac{1}{Ro}\widehat{\boldsymbol{z}}\times\boldsymbol{u}$$
$$= -Eu\left(\boldsymbol{\nabla}+\overline{\boldsymbol{\nabla}}\right)p + M\left(\boldsymbol{B}\cdot\boldsymbol{\nabla}+\boldsymbol{B}\cdot\overline{\boldsymbol{\nabla}}\right)\boldsymbol{B} + \Gamma\,\theta\widehat{\boldsymbol{z}} + \frac{1}{Re}\left(\nabla^2+\overline{\nabla}^2\right)\boldsymbol{u}, \tag{2.18}$$

$$\left(\partial_t + \frac{1}{A_\tau}\partial_\tau + \frac{1}{A_T}\partial_T \right)\theta + \boldsymbol{\nabla}\cdot(\theta\boldsymbol{u}) + \overline{\boldsymbol{\nabla}}\cdot(\theta\boldsymbol{u}) = \frac{1}{Pe}\left(\nabla^2+\overline{\nabla}^2\right)\theta, \tag{2.19}$$

$$\left(\partial_t + \frac{1}{A_\tau}\partial_\tau + \frac{1}{A_T}\partial_T \right)\boldsymbol{B} = \boldsymbol{\nabla}\times(\boldsymbol{u}\times\boldsymbol{B}) + \overline{\boldsymbol{\nabla}}\times(\boldsymbol{u}\times\boldsymbol{B}) + \frac{1}{Rm}\left(\nabla^2+\overline{\nabla}^2\right)\boldsymbol{B}, \tag{2.20}$$

$$\left(\boldsymbol{\nabla}+\overline{\boldsymbol{\nabla}}\right)\cdot\boldsymbol{u} = 0, \quad \left(\boldsymbol{\nabla}+\overline{\boldsymbol{\nabla}}\right)\cdot\boldsymbol{B} = 0. \tag{2.21a,b}$$

The superscript ‘T’ appearing on some of the velocity vectors denotes a transpose.

Averaging the equations over fast temporal and spatial scales ($\boldsymbol{x}$, t) results in the mean equations

$$\left(\frac{1}{A_\tau}\partial_\tau + \frac{1}{A_T}\partial_T \right)\overline{\boldsymbol{u}} + \overline{\boldsymbol{\nabla}}\cdot\left(\overline{\boldsymbol{u}}(\overline{\boldsymbol{u}})^{\mathrm{T}}\right) + \overline{\boldsymbol{\nabla}}\cdot\overline{(\boldsymbol{u}'(\boldsymbol{u}')^{\mathrm{T}})} + \frac{1}{Ro}\widehat{\boldsymbol{z}}\times\overline{\boldsymbol{u}}$$
$$= -Eu\overline{\boldsymbol{\nabla}}\overline{p} + M\overline{\boldsymbol{F}}_L + \Gamma\,\overline{\theta}\,\widehat{\boldsymbol{z}} + \frac{1}{Re}\overline{\nabla}^2\overline{\boldsymbol{u}}, \tag{2.22}$$

$$\left(\frac{1}{A_\tau}\partial_\tau + \frac{1}{A_T}\partial_T \right)\overline{\theta} + \overline{\boldsymbol{\nabla}}\cdot\left(\overline{\theta}\,\overline{\boldsymbol{u}}\right) + \overline{\boldsymbol{\nabla}}\cdot\overline{(\theta'\boldsymbol{u}')} = \frac{1}{Pe}\overline{\nabla}^2\overline{\theta}, \tag{2.23}$$

$$\left(\frac{1}{A_\tau}\partial_\tau + \frac{1}{A_T}\partial_T \right)\overline{\boldsymbol{B}} = \overline{\boldsymbol{\nabla}}\times(\overline{\boldsymbol{u}}\times\overline{\boldsymbol{B}}) + \overline{\boldsymbol{\nabla}}\times\overline{(\boldsymbol{u}'\times\boldsymbol{b}')} + \frac{1}{Rm}\overline{\nabla}^2\overline{\boldsymbol{B}}, \tag{2.24}$$

$$\overline{\boldsymbol{\nabla}}\cdot\overline{\boldsymbol{u}} = 0, \quad \overline{\boldsymbol{\nabla}}\cdot\overline{\boldsymbol{B}} = 0, \tag{2.25a,b}$$

where the mean Lorentz force is $\overline{\boldsymbol{F}}_L = \overline{\boldsymbol{B}}\cdot\overline{\boldsymbol{\nabla}}\,\overline{\boldsymbol{B}} + \overline{\boldsymbol{b}'\cdot\boldsymbol{\nabla}\boldsymbol{b}'}$.

The fluctuating equations are found by subtracting the mean equations from the full equations to give

$$\left(\partial_t + \frac{1}{A_\tau}\partial_\tau + \frac{1}{A_T}\partial_T\right)\boldsymbol{u}' + \boldsymbol{\nabla}\cdot(\boldsymbol{u}\boldsymbol{u}^{\mathrm{T}}) + \overline{\boldsymbol{\nabla}}\cdot(\boldsymbol{u}'\overline{\boldsymbol{u}}^{\mathrm{T}}) + \overline{\boldsymbol{\nabla}}\cdot(\boldsymbol{u}(\boldsymbol{u}')^{\mathrm{T}}) - \overline{\boldsymbol{\nabla}}\cdot\overline{(\boldsymbol{u}'(\boldsymbol{u}')^{\mathrm{T}})} + \frac{1}{Ro}\widehat{\boldsymbol{z}}\times\boldsymbol{u}' = -Eu\,\left(\overline{\boldsymbol{\nabla}}+\boldsymbol{\nabla}\right)p' + M\boldsymbol{F}_L' + \Gamma\,\theta'\widehat{\boldsymbol{z}} + \frac{1}{Re}(\nabla^2+\overline{\nabla}^2)\boldsymbol{u}', \tag{2.26}$$

$$\left(\partial_t + \frac{1}{A_\tau}\partial_\tau + \frac{1}{A_T}\partial_T\right)\theta' + \boldsymbol{u}'\cdot\overline{\boldsymbol{\nabla}}\,\overline{\theta} + \overline{\boldsymbol{u}}\cdot\boldsymbol{\nabla}\theta' + \overline{\boldsymbol{\nabla}}\cdot\left(\boldsymbol{u}'\theta'\right) - \overline{\boldsymbol{\nabla}}\cdot\overline{(\boldsymbol{u}'\theta')} = \frac{1}{Pe}\left(\nabla^2+\overline{\nabla}^2\right)\theta', \tag{2.27}$$

$$\left(\partial_t + \frac{1}{A_\tau}\partial_\tau + \frac{1}{A_T}\partial_T\right)\boldsymbol{b}' = \overline{\boldsymbol{\nabla}}\times(\overline{\boldsymbol{u}}\times\boldsymbol{b}') + \overline{\boldsymbol{\nabla}}\times(\boldsymbol{u}'\times\overline{\boldsymbol{B}}) + \overline{\boldsymbol{\nabla}}\times(\boldsymbol{u}'\times\boldsymbol{b}') - \overline{\boldsymbol{\nabla}}\times\overline{(\boldsymbol{u}'\times\boldsymbol{b}')} + \boldsymbol{\nabla}\times(\overline{\boldsymbol{u}}\times\boldsymbol{b}') + \boldsymbol{\nabla}\times(\boldsymbol{u}'\times\overline{\boldsymbol{B}}) + \boldsymbol{\nabla}\times(\boldsymbol{u}'\times\boldsymbol{b}') + \frac{1}{Rm}\nabla^2 + \overline{\nabla}^2\boldsymbol{b}', \tag{2.28}$$

$$\left(\overline{\boldsymbol{\nabla}}+\boldsymbol{\nabla}\right)\cdot\boldsymbol{u}' = 0, \quad \left(\overline{\boldsymbol{\nabla}}+\boldsymbol{\nabla}\right)\cdot\boldsymbol{b}' = 0, \tag{2.29a,b}$$

where the fluctuating Lorentz force is

$$\boldsymbol{F}_L' = \overline{\boldsymbol{B}}\cdot\boldsymbol{\nabla}\boldsymbol{b}' + \boldsymbol{b}'\cdot\overline{\boldsymbol{\nabla}}\,\overline{\boldsymbol{B}} + \boldsymbol{b}'\cdot\boldsymbol{\nabla}\boldsymbol{b}' - \overline{\boldsymbol{b}'\cdot\boldsymbol{\nabla}\boldsymbol{b}'}. \tag{2.30}$$

2.2. *Asymptotics*

We note that up to this point, no approximations have been made; the equations have simply been split up into mean and fluctuating components. In the present work we are interested in the development of a multiscale dynamo model that preserves geostrophic balance on the small (fluctuating) scales. Because the fluctuating and mean dynamics are coupled, *a posteriori* we find that the large-scales are required to also be geostrophically balanced in the horizontal directions, and hydrostatic in the vertical direction, resulting in a thermal wind balance. The relevant asymptotic limit for the present model is therefore the small Rossby number limit, $Ro \equiv \epsilon \to 0$.

When constructing an asymptotic model with more than one small (or large) parameter, it is necessary to establish the so-called distinguished limits, or the asymptotic scaling relationships between the various parameters. In the present context this implies that we must relate, in an order of magnitude sense, both the non-dimensional parameters introduced in (2.5) and (2.6), as well as the aspect ratios defined by (2.17), to the Rossby number ϵ. This procedure is well known, and hinges on the identification of dominant balances in the governing equations that will allow for a mathematically and physically meaningful reduced model; by definition the procedure is circular in nature (e.g. see Bender & Orszag 2010). In this regard, to ensure geostrophically balanced convection on the small scales, we follow § 2 of Sprague *et al.* (2006) and employ the following distinguished limits

$$A_Z = \epsilon^{-1}, \quad A_T = \epsilon^{-2}, \quad Eu = \epsilon^{-2}, \quad \Gamma = \epsilon^{-1}\widetilde{\Gamma}, \quad Re = O(1), \quad Pe = O(1), \tag{2.31a–f}$$

where the reduced buoyancy number $\widetilde{\Gamma} = O(1)$. We note that with these scalings, the small-scale velocity field $\boldsymbol{u}'$ is $O(1)$. We further assume the large-scale pressure $\overline{p}$, magnetic field $\overline{\boldsymbol{B}}$ and temperature $\overline{\theta}$ to also be $O(1)$ in magnitude.

The dimensional scales employed in the dimensionless parameters given by (2.5) and (2.6) will be those of the largest amplitude. For convenience, the parameters Eu, Γ, and M will therefore be based on 'mixed' scales in our asymptotic development in the sense that the pressure, temperature and magnetic field amplitudes are based on the large-scale quantities $(\overline{p}, \overline{\boldsymbol{B}}, \overline{\theta})$, whereas the velocity scale is based on $\boldsymbol{u}'$. In this sense, the dimensional magnitudes of these variables is absorbed in the various non-dimensional parameters. In § 3.4 we briefly discuss the renormalization of these non-dimensional parameters such that they are based on equivalent (large or small) dimensional scales.

It now remains to determine the distinguished limits of A_X, A_τ, M and Rm. To provide some explanation as to how these limits are achieved we examine various terms in the governing equations that we wish to retain in the final reduced model. The distinguished limit of A_X can be determined by restricting the large-scale horizontal motions to be geostrophically balanced; utilizing (2.22) we have

$$\frac{1}{\epsilon}\widehat{\boldsymbol{z}} \times \overline{\boldsymbol{u}} \approx -\frac{1}{\epsilon^2 A_X}\overline{\boldsymbol{\nabla}}_x \overline{p}, \tag{2.32}$$

where $\boldsymbol{\nabla}_X = (\partial_X, \partial_Y, 0)$. We then get

$$\overline{\boldsymbol{u}} \sim (\epsilon A_X)^{-1}. \tag{2.33}$$

Turning our attention to the mean temperature equation (2.23), we wish to keep horizontal advection of the mean temperature by the mean velocity field at the same order as the temporal evolution of the mean temperature so that

$$\epsilon^2 \partial_T \overline{\theta} \sim \frac{1}{A_X}\overline{\boldsymbol{u}} \cdot \boldsymbol{\nabla}_X \overline{\theta}, \tag{2.34}$$

which leads to

$$\overline{\boldsymbol{u}} \sim \epsilon^2 A_X. \tag{2.35}$$

Combining (2.33) with (2.35) then shows that we must have

$$A_X = \epsilon^{-3/2}, \tag{2.36}$$

and so $\overline{\boldsymbol{u}} = O(\epsilon^{1/2})$. We note that this also implies large-scale horizontal gradients are smaller than the corresponding large-scale vertical gradients by a factor $A_Z/A_X = \epsilon^{1/2}$.

The distinguished limits of A_τ, M, and Rm are determined by examining the influence of the magnetic field. To generate dynamo action on the large scales via coupling with the fluctuating dynamics, we necessarily require the presence of the second term on the right-hand side of (2.24), where $\overline{(\boldsymbol{u}' \times \boldsymbol{b}')}$ is referred to as the mean electromotive force, or mean emf (e.g. Parker 1955; Steenbeck & Krause 1966; Steenbeck, Krause & Rädler 1966; Moffatt 1978). Utilizing the above scalings for A_X and $\overline{\boldsymbol{u}}$, and retaining only the largest terms, the order of magnitude of each term present in the mean induction equation is then

$$\frac{\overline{\boldsymbol{B}}}{A_\tau} : \epsilon^{3/2}\overline{\boldsymbol{B}} : \epsilon \boldsymbol{b}' : \frac{\epsilon^2}{Rm}\overline{\boldsymbol{B}}, \tag{2.37}$$

where we recall that the fluctuating velocity field is order one, consistent with Sprague *et al.* (2006). The colons used above are meant to signify that we are making a comparison of the magnitude of each term in the original governing equation and we have retained $\overline{\boldsymbol{B}} = O(1)$ for clarity in identifying the various terms. To retain time-dependence of the mean magnetic field, we require that the first and third terms be of the same magnitude such that

$$\overline{\boldsymbol{B}} \sim \epsilon A_\tau \boldsymbol{b}'. \tag{2.38}$$

By noting that all the large-scale gradients are small relative to the small-scale gradients, the order of magnitude of the four largest terms in the fluctuating induction equation (2.28) (the first on the left-hand side, and the fifth, sixth and eighth terms on the right-hand side) are

$$\boldsymbol{b}' : \overline{\boldsymbol{B}} : \boldsymbol{b}' : \frac{\boldsymbol{b}'}{Rm}. \tag{2.39}$$

We require that ohmic dissipation is present in the final model, at least with respect to the small scales. The largest term present above would then be that associated with stretching the mean magnetic field such that

$$\overline{\boldsymbol{B}} \sim \frac{\boldsymbol{b}'}{Rm}, \tag{2.40}$$

i.e. $\boldsymbol{b}' \sim Rm$. Finally, because we are investigating dynamo action, we require that the Lorentz force enter the small-scale momentum dynamics. From Sprague *et al.* (2006), and examination of (2.26), we know that this requires

$$M\overline{\boldsymbol{B}}\boldsymbol{b}' = O(1). \tag{2.41}$$

Combining this scaling with (2.40) yields

$$M = O(Rm^{-1}). \tag{2.42}$$

We can now determine the size of Rm by returning to the mean induction equation. For large-scale dynamo action, magnetic diffusion cannot dominate the mean emf so that comparison of the third and fourth terms, respectively, given in (2.37) yields

$$\epsilon \boldsymbol{b}' \gtrsim \frac{\epsilon^2}{Rm}\overline{\boldsymbol{B}}. \tag{2.43}$$

Using the above scaling with (2.40) shows that

$$Rm \geqslant \epsilon^{1/2}, \tag{2.44}$$

with the lower bound being the case $Rm = O(\epsilon^{1/2})$. The particular distinguished limit taken for Rm will in turn determine the size of the magnetic Prandtl number since $Rm = RePm$. Taking $Rm = O(\epsilon^{1/2})$ corresponds to the low Pm limit since $Re = O(1)$. An alternative scaling would be to take $Rm = O(1)$ and thus $Pm = O(1)$. The main focus of the present manuscript is for the $Rm = O(\epsilon^{1/2})$ limit given that it ties directly to the CSDM and is implicitly low Pm. We also present the form of the governing equations for the $Rm = O(1)$ case, but note additional complications that arise in this limit which will require future analysis that is beyond the scope of the present work.

2.2.1. *The $Rm = O(\epsilon^{1/2})$ limit*

Here we take $Rm = \epsilon^{1/2}\widetilde{Rm}$, where we define the reduced magnetic Reynolds number $\widetilde{Rm} = O(1)$. Returning to relationships (2.38) and (2.42) we can now define the distinguished limits of A_τ and M as

$$A_\tau = \epsilon^{-3/2}, \quad M = \epsilon^{-1/2}, \tag{2.45}$$

showing that three disparate time scales are now present in the QGDM.

With our distinguished limits defined, we now follow CS72 and expand all variables in powers of $\epsilon^{1/2}$, e.g.

$$\boldsymbol{u} = \overline{\boldsymbol{u}}_0 + \boldsymbol{u}'_0 + \epsilon^{1/2}\left(\overline{\boldsymbol{u}}_{1/2} + \boldsymbol{u}'_{1/2}\right) + \epsilon\left(\overline{\boldsymbol{u}}_1 + \boldsymbol{u}'_1\right) + \cdots . \tag{2.46}$$

Plugging the perturbation expansions into the governing equations and collecting terms of equal magnitude, the leading order solenoidal conditions on the mean velocity and magnetic fields gives

$$\partial_Z \overline{w}_0 = 0, \quad \partial_Z \overline{B}_0^{(z)} = 0. \tag{2.47a,b}$$

Owing to our use of impenetrable, perfectly conducting boundary conditions we require $\overline{w}_0 = \overline{B}_0^{(z)} \equiv 0$. At the next order the solenoidal conditions yield

$$\boldsymbol{\nabla}_X \cdot \overline{\boldsymbol{u}}_0 + \partial_Z \overline{w}_{1/2} = 0, \quad \boldsymbol{\nabla}_X \cdot \overline{\boldsymbol{B}}_0 + \partial_Z \overline{B}_{1/2}^{(z)} = 0. \tag{2.48a,b}$$

At order $O(\epsilon^{-1})$ the horizontal mean momentum equation gives

$$\widehat{\boldsymbol{z}} \times \overline{\boldsymbol{u}}_0 = 0, \tag{2.49}$$

showing that $\overline{\boldsymbol{u}}_0 \equiv 0$. Utilizing continuity it follows that $\overline{w}_{1/2} \equiv 0$. The next three orders of the mean horizontal momentum equation are then geostrophically balanced,

$$\widehat{\boldsymbol{z}} \times \overline{\boldsymbol{u}}_i = -\boldsymbol{\nabla}_X \overline{p}_{i-1/2}, \quad i = \tfrac{1}{2}, 1, \tfrac{3}{2}. \tag{2.50}$$

Carrying the expansion out to $O(\epsilon)$ shows that $\overline{\boldsymbol{u}}_2$ is magnetostrophically balanced,

$$\widehat{\boldsymbol{z}} \times \overline{\boldsymbol{u}}_2 = -\boldsymbol{\nabla}_X \overline{p}_{3/2} + \overline{\boldsymbol{B}}_0 \cdot \nabla_X \overline{\boldsymbol{B}}_0 + \overline{B}_{1/2}^{(z)} \partial_Z \overline{\boldsymbol{B}}_0. \tag{2.51}$$

The vertical mean momentum equation yields hydrostatic balance for the first four orders,

$$\partial_Z \overline{p}_i = \widetilde{\Gamma} \overline{\theta}_i, \quad i = 0, \tfrac{1}{2}, 1, \tfrac{3}{2}. \tag{2.52}$$

Taking the curl of (2.50) shows that

$$\boldsymbol{\nabla}_X \cdot \overline{\boldsymbol{u}}_i = 0, \quad i = 0, \tfrac{1}{2}, 1, \tfrac{3}{2} \tag{2.53}$$

and thus $\overline{w}_i \equiv 0$ for $i = 0, \ldots, 2$. Combining equation (2.50) for $i = 1/2$ and (2.52) for $i = 0$ we then obtain the well-known thermal wind relations

$$\partial_Z \overline{v}_{1/2} = \widetilde{\Gamma} \partial_X \overline{\theta}_0, \quad \partial_Z \overline{u}_{1/2} = -\widetilde{\Gamma} \partial_Y \overline{\theta}_0. \tag{2.54a,b}$$

Because the large-scale velocity field is horizontally divergence free we can define the large-scale geostrophic stream function as $\overline{\Psi}_{1/2} \equiv \overline{p}_0$ such that

$$\overline{\boldsymbol{u}}_{1/2} = -\overline{\boldsymbol{\nabla}} \times \overline{\Psi}_{1/2}\widehat{\boldsymbol{z}}. \tag{2.55}$$

We note that the mathematical structure of the thermal wind relations (2.54) yields any barotropic (i.e. depth invariant) geostrophic large-scale flow undetermined given that $\overline{\boldsymbol{u}}_{1/2}$ only appears with first-order Z-derivatives. In some instances this barotropic flow plays a significant dynamical role and must be consistently determined via an evolution equation (cf. Dolaptchiev & Klein 2009). However, in the present work the evolution equation for such a mode enters at a much higher, subdominant order, and we do not consider it any further.

Proceeding to the mean horizontal induction equation, at $O(\epsilon)$ we have

$$0 = \widehat{\boldsymbol{z}} \times \partial_Z \overline{\left(\boldsymbol{u}_0' \times \boldsymbol{b}_0'\right)}, \tag{2.56}$$

which, in general, requires that $\boldsymbol{b}_0' \equiv 0$. Alternatively, from the scaling relationship given by (2.40), we require that $\boldsymbol{b}' = O(\epsilon^{1/2})$ if $\overline{\boldsymbol{B}} = O(1)$. At $O(\epsilon^{3/2})$ we get

$$\partial_\tau \overline{\boldsymbol{B}}_0^{\perp} = \widehat{\boldsymbol{z}} \times \partial_Z \overline{\left(\boldsymbol{u}_0' \times \boldsymbol{b}_{1/2}'\right)} + \frac{1}{\widetilde{Rm}} \partial_Z^2 \overline{\boldsymbol{B}}_0^{\perp}, \tag{2.57}$$

where $\overline{\boldsymbol{B}}_0^{\perp} \equiv (\overline{B}_0^{(x)}, \overline{B}_0^{(y)}, 0)$. The leading order vertical component of the mean induction equation becomes

$$\partial_\tau \overline{B}_{1/2}^{(z)} = \widehat{\boldsymbol{y}} \cdot \partial_X \overline{\left(\boldsymbol{u}_0' \times \boldsymbol{b}_{1/2}'\right)} - \widehat{\boldsymbol{x}} \cdot \partial_Y \overline{\left(\boldsymbol{u}_0' \times \boldsymbol{b}_{1/2}'\right)} + \frac{1}{\widetilde{Rm}} \partial_Z^2 \overline{B}_{1/2}^{(z)}, \tag{2.58}$$

where we see that a non-trivial mean vertical magnetic field requires the presence of a large-scale horizontal modulation in the sense that $\overline{B}_{1/2}^{(z)} \equiv 0$ if $\partial_X = \partial_Y \equiv 0$ (this fact can also be seen from (2.48)). The fluctuating induction equation then gives

$$0 = \overline{\boldsymbol{B}}_0^{\perp} \cdot \boldsymbol{\nabla}_\perp \boldsymbol{u}_0' + \frac{1}{\widetilde{Rm}} \nabla^2 \boldsymbol{b}_{1/2}', \tag{2.59}$$

where $\boldsymbol{\nabla}_\perp = \left(\partial_x, \partial_y, 0\right)$.

The leading order mean temperature equation gives

$$\partial_Z \overline{\left(w_0' \theta_0'\right)} = 0, \tag{2.60}$$

showing that $\theta_0' \equiv 0$. At the next order we have

$$\partial_\tau \overline{\theta}_0 + \partial_Z \overline{\left(w_0' \theta_{1/2}'\right)} = 0, \tag{2.61}$$

again showing that $\theta_{1/2}' \equiv 0$ and thus $\partial_\tau \overline{\theta}_0 \equiv 0$. Finally, we have

$$\partial_\tau \overline{\theta}_{1/2} + \partial_T \overline{\theta}_0 + \overline{\boldsymbol{u}}_{1/2} \cdot \boldsymbol{\nabla}_X \overline{\theta}_0 + \partial_Z \overline{\left(w_0' \theta_1'\right)} = \frac{1}{Pe} \partial_Z^2 \overline{\theta}_0. \tag{2.62}$$

To avoid secular growth of the mean temperature on the time scale τ we set $\partial_\tau \overline{\theta}_{1/2} \equiv 0$; the mean heat equation then becomes

$$\partial_T \overline{\theta}_0 + \overline{\boldsymbol{u}}_{1/2} \cdot \boldsymbol{\nabla}_X \overline{\theta}_0 + \partial_Z \overline{\left(w_0' \theta_1'\right)} = \frac{1}{Pe} \partial_Z^2 \overline{\theta}_0. \tag{2.63}$$

Alternatively, one can average equation (2.62) over the time scale τ to obtain an equation identical to (2.63), with the exception that the averages must then be interpreted as occurring over $(\boldsymbol{x}, t, \tau)$. At $O(\epsilon)$ the fluctuating temperature equation is

$$\partial_t \theta_1' + \boldsymbol{u}_0' \cdot \boldsymbol{\nabla}_\perp \theta_1' + w_0' \partial_Z \overline{\theta}_0 = \frac{1}{Pe} \nabla^2 \theta_1'. \tag{2.64}$$

At $O(\epsilon^{-2})$ and $O(\epsilon^{-3/2})$ the fluctuating momentum equation yields, respectively

$$\boldsymbol{\nabla} p_i' = 0, \quad i = 0, \tfrac{1}{2} \tag{2.65}$$

showing that $p_0' = p_{1/2}' \equiv 0$. Geostrophy occurs at $O(\epsilon^{-1})$ and $O(\epsilon^{-1/2})$

$$\widehat{\boldsymbol{z}} \times \boldsymbol{u}_i' = -\boldsymbol{\nabla} p_{i+1}', \quad i = 0, \tfrac{1}{2}. \tag{2.66}$$

Additionally, mass conservation at $O(1)$ and $O(\epsilon^{1/2})$ gives

$$\boldsymbol{\nabla} \cdot \boldsymbol{u}_i' = 0, \quad i = 0, \tfrac{1}{2}, \tag{2.67}$$

which, along with (2.66), yields the Proudman–Taylor theorem acting over the small vertical scale z

$$\partial_z \left(\boldsymbol{u}_i', p_{i+1}'\right) = 0, \quad i = 0, \tfrac{1}{2}. \tag{2.68}$$

It is natural to wonder why the Proudman–Taylor theorem is satisfied over the small scale z and not the axial domain scale Z. It is well known from the linear theory of rapidly rotating convection that the leading order, geostrophically balanced convection possesses order one variations over the height of the fluid layer (our large-scale coordinate Z) (Chandrasekhar 1961). The only way to be consistent with the Proudman–Taylor theorem, whilst allowing convection to occur on the axial domain scale, is for it to be satisfied over the small vertical scale z. We recall that this is the same scale as the horizontal convective scales (x, y). This fact appears to be first noted by Stewartson & Cheng (1979); apart from the presence of viscous and body forces in the present work, their vorticity (2.7*b*) and vertical momentum (2.7*a*) equations are identical to our small-scale counterparts given by (2.70) and (2.71).

The prognostic momentum equation then appears at $O(1)$

$$\partial_t \boldsymbol{u}_0' + \boldsymbol{u}_0' \cdot \boldsymbol{\nabla}_\perp \boldsymbol{u}_0' + \widehat{\boldsymbol{z}} \times \boldsymbol{u}_1' = -\boldsymbol{\nabla} p_2' - \partial_Z p_1' \widehat{\boldsymbol{z}} + \widetilde{\Gamma} \theta_1' \widehat{\boldsymbol{z}} + \overline{\boldsymbol{B}}_0 \cdot \boldsymbol{\nabla}_\perp \boldsymbol{b}_{1/2}' + \frac{1}{Re} \nabla_\perp^2 \boldsymbol{u}_0', \tag{2.69}$$

where we note the key distinction with the CSDM is the simultaneous appearance of both the advection and Lorentz force terms. In light of (2.66), we can define the small-scale geostrophic stream function as $\psi_0' \equiv p_1'$ such that the fluctuating horizontal velocity field is given by $(u_0', v_0') = (-\partial_y \psi_0', \partial_x \psi_0')$. As noted by Sprague *et al.* (2006), (2.69) still depends upon the small vertical scale z; to avoid secular growth on this scale it is necessary to impose solvability conditions. These solvability conditions

amount to operating on (2.69) with $\widehat{\boldsymbol{z}}\cdot\boldsymbol{\nabla}\times$ and $\widehat{\boldsymbol{z}}\cdot$, respectively, and averaging over the small vertical scale z to obtain (see also Calkins, Julien & Marti 2013)

$$\partial_t\nabla_\perp^2\psi_0' + \mathrm{J}(\psi_0', \nabla_\perp^2\psi_0') - \partial_Z w_0' = \widehat{\boldsymbol{z}}\cdot\boldsymbol{\nabla}\times\left(\overline{\boldsymbol{B}}_0\cdot\boldsymbol{\nabla}_\perp\langle\boldsymbol{b}_{1/2}'\rangle\right) + \frac{1}{Re}\nabla_\perp^4\psi_0', \tag{2.70}$$

$$\partial_t w_0' + \mathrm{J}(\psi_0', w_0') + \partial_Z\psi_0' = \widetilde{\Gamma}\langle\theta_1'\rangle + \widehat{\boldsymbol{z}}\cdot\left(\overline{\boldsymbol{B}}_0\cdot\boldsymbol{\nabla}_\perp\langle\boldsymbol{b}_{1/2}'\rangle\right) + \frac{1}{Re}\nabla_\perp^2 w_0', \tag{2.71}$$

where $\mathrm{J}(F, G) = \partial_x F\partial_y G - \partial_x G\partial_y F$, the angled brackets denote a spatial average over z and the vertical vorticity is $\zeta_0 = \nabla_\perp^2\psi_0'$.

Upon rescaling the velocity with the small-scale viscous diffusion time such that $U = \nu/L$, the closed set of reduced equations is given by

$$\overline{\boldsymbol{u}}_{1/2} = -\overline{\boldsymbol{\nabla}}\times\overline{\Psi}_{1/2}\widehat{\boldsymbol{z}}, \tag{2.72}$$

$$\partial_Z\overline{\Psi}_{1/2} = \frac{\widetilde{Ra}}{Pr}\overline{\theta}_0, \tag{2.73}$$

$$\partial_T\overline{\theta}_0 + \overline{\boldsymbol{u}}_{1/2}\cdot\boldsymbol{\nabla}_X\overline{\theta}_0 + \partial_Z\overline{\left(w_0'\theta_1'\right)} = \frac{1}{Pr}\partial_Z^2\overline{\theta}_0, \tag{2.74}$$

$$\partial_\tau\overline{\boldsymbol{B}}_0^\perp = \widehat{\boldsymbol{z}}\times\partial_Z\overline{\left(\boldsymbol{u}_0'\times\langle\boldsymbol{b}_{1/2}'\rangle\right)} + \frac{1}{\widetilde{Pm}}\partial_Z^2\overline{\boldsymbol{B}}_0^\perp, \tag{2.75}$$

$$\partial_\tau\overline{B}_{1/2}^{(z)} = \widehat{\boldsymbol{y}}\cdot\partial_X\overline{\left(\boldsymbol{u}_0'\times\langle\boldsymbol{b}_{1/2}'\rangle\right)} - \widehat{\boldsymbol{x}}\cdot\partial_Y\overline{\left(\boldsymbol{u}_0'\times\langle\boldsymbol{b}_{1/2}'\rangle\right)} + \frac{1}{\widetilde{Pm}}\partial_Z^2\overline{B}_{1/2}^{(z)}, \tag{2.76}$$

$$\partial_X\overline{B}_0^{(x)} + \partial_Y\overline{B}_0^{(y)} + \partial_Z\overline{B}_{1/2}^{(z)} = 0, \tag{2.77}$$

$$\partial_t\nabla_\perp^2\psi_0' + \mathrm{J}(\psi_0', \nabla_\perp^2\psi_0') - \partial_Z w_0' = \widehat{\boldsymbol{z}}\cdot\boldsymbol{\nabla}\times\left(\overline{\boldsymbol{B}}_0\cdot\boldsymbol{\nabla}_\perp\langle\boldsymbol{b}_{1/2}'\rangle\right) + \nabla_\perp^4\psi_0', \tag{2.78}$$

$$\partial_t w_0' + \mathrm{J}(\psi_0', w_0') + \partial_Z\psi_0' = \frac{\widetilde{Ra}}{Pr}\langle\theta_1'\rangle + \overline{\boldsymbol{B}}_0\cdot\boldsymbol{\nabla}_\perp\langle b_{1/2}'^{(z)}\rangle + \nabla_\perp^2 w_0', \tag{2.79}$$

$$\partial_t\langle\theta_1'\rangle + \mathrm{J}(\psi_0', \langle\theta_1'\rangle) + w_0'\partial_Z\overline{\theta}_0 = \frac{1}{Pr}\nabla_\perp^2\langle\theta_1'\rangle, \tag{2.80}$$

$$0 = \overline{\boldsymbol{B}}_0^\perp\cdot\boldsymbol{\nabla}_\perp\boldsymbol{u}_0' + \frac{1}{\widetilde{Pm}}\nabla_\perp^2\langle\boldsymbol{b}_{1/2}'\rangle, \tag{2.81}$$

$$\partial_x\langle b_{1/2}'^{(x)}\rangle + \partial_y\langle b_{1/2}'^{(y)}\rangle = 0. \tag{2.82}$$

The reduced Rayleigh number, consistent with the linear theory of rapidly rotating convection (Chandrasekhar 1961), is defined by $\widetilde{Ra} = \epsilon^4 Ra_H = Ek^{4/3}Ra_H$, where the Rayleigh number is given by

$$Ra_H = \frac{g\alpha\Delta T H^3}{\nu\kappa}. \tag{2.83}$$

The reduced magnetic Prandtl number appearing in the above system is defined by $\widetilde{Pm} = \epsilon^{1/2}Pm = O(1)$.

The final reduced system is tenth order in the large-scale vertical coordinate Z. Written in terms of the reduced variables, the ten boundary conditions become

$$\overline{\theta}_0 = \begin{cases} 1 & \text{at } Z = 0, \\ 0 & \text{at } Z = 1, \end{cases} \tag{2.84}$$

$$\partial_Z\overline{B}_0^{(x)} = \partial_Z\overline{B}_0^{(y)} = \overline{B}_{1/2}^{(z)} = w_0' = 0 \quad \text{at } Z = 0,\ 1. \tag{2.85}$$

Taking the horizontal divergence of (2.81) shows that (2.82) is identically satisfied since the geostrophic velocity field is horizontally divergence free. Although direct imposition of (vertical) boundary conditions is not possible with (2.81) given the lack of Z-derivatives with respect to $\langle \boldsymbol{b}'_{1/2} \rangle$, evaluating this equation at the boundaries $Z = 0$ and $Z = 1$ shows that the fluctuating magnetic field implicitly satisfies the magnetic boundary conditions as long as boundary conditions can be explicitly imposed on the mean magnetic field; this result holds regardless of the specific magnetic boundary conditions employed.

Although the details of obtaining numerical solutions to the reduced system are beyond the scope of the present work, we mention that several approaches have been developed to handle both multiple scales in space and time. In particular, so-called heterogeneous multiscale methods (HMM) have been successfully applied to numerous applications (Weinan *et al.* 2007). For example, a modified form of HMM has recently been developed for simulating a multiscale model of upper ocean Langmuir circulation (Chini, Julien & Knobloch 2009; Malecha, Chini & Julien 2014). In addition, Haut & Wingate (2014) have developed a time stepping algorithm for problems with temporal scale separation which may be of use for the present model.

2.2.2. *The* $Rm = O(1)$ *Limit*

The asymptotic development of the $Rm = O(1)$ parallels that for the $Rm = O(\epsilon^{1/2})$ case given above. For this reason we omit many of the details and focus only on the differences between the two limiting cases. We emphasize again that the $Rm = O(1)$ limit corresponds to $Pm = O(1)$ since $Re = O(1)$. Consideration of relationships (2.38) and (2.42) with $Rm = O(1)$ shows that we must have

$$A_\tau = \epsilon^{-1}, \quad M = O(1). \tag{2.86a,b}$$

In addition, relationship (2.40) shows that the mean and fluctuating magnetic fields are now of the same order, i.e. $\overline{\boldsymbol{B}} \sim \boldsymbol{b}'$. The main differences that occur in the final reduced model for the $Rm = O(1)$ case are that the Lorentz force becomes $\overline{\boldsymbol{B}}_0 \cdot \boldsymbol{\nabla}_\perp \boldsymbol{b}'_0 + \boldsymbol{b}'_0 \cdot \boldsymbol{\nabla} \boldsymbol{b}'_0$ and the leading order induction equations are given by

$$\partial_\tau \overline{\boldsymbol{B}}_0^\perp = \widehat{\boldsymbol{z}} \times \partial_Z \overline{\left(\boldsymbol{u}'_0 \times \langle \boldsymbol{b}'_0 \rangle \right)}, \tag{2.87}$$

$$\partial_\tau \overline{B}_{1/2}^{(z)} = \widehat{\boldsymbol{y}} \cdot \partial_X \overline{\left(\boldsymbol{u}'_0 \times \langle \boldsymbol{b}'_0 \rangle \right)} - \widehat{\boldsymbol{x}} \cdot \partial_Y \overline{\left(\boldsymbol{u}'_0 \times \langle \boldsymbol{b}'_0 \rangle \right)}, \tag{2.88}$$

$$\partial_t \langle \boldsymbol{b}'_0 \rangle + \boldsymbol{u}'_0 \cdot \boldsymbol{\nabla}_\perp \langle \boldsymbol{b}'_0 \rangle = \overline{\boldsymbol{B}}_0^\perp \cdot \boldsymbol{\nabla}_\perp \boldsymbol{u}'_0 + \frac{1}{Pm} \nabla_\perp^2 \langle \boldsymbol{b}'_0 \rangle. \tag{2.89}$$

The boundary conditions for the $Rm = O(1)$ case are identical to those given by (2.84)–(2.85). Equations (2.87)–(2.88) shows that due to the absence of Z-derivatives, no mean magnetic field boundary conditions can be satisfied without the inclusion of magnetic boundary layers. Further work is necessary to examine the effects of these boundary layers.

3. Discussion

3.1. *The* $Rm = O(\epsilon^{1/2})$ *limit*

Here we reiterate some of the key features of the low magnetic Prandtl number QGDM and interpret the various terms in the equation set (2.72)–(2.82). Equations (2.72)–(2.73) are statements of geostrophic balance and hydrostatic balance on the

large horizontal and vertical scales, respectively. Importantly, these equations are diagnostic since they contain no information about the temporal evolution; this is a well-known characteristic and the prognostic dynamics are obtained from the mean heat equation (2.74). From (2.72) we see that viscous diffusion is negligible on the large scales. The mean heat equation given by (2.74) shows that the mean velocity field is strong enough to allow advection of the mean temperature over the large horizontal scales (X, Y) as shown by the second term on the left-hand side, whereas the third term represents the influence of convective feedback from the fluctuating scales back onto the large-scales. Additionally, the presence of large-scale thermal diffusion over the vertical dimension is represented by the term on the right-hand side of (2.74).

Both of the mean induction equations given by (2.75) and (2.76) contain time-dependence, the mean emf that represents the feedback from fluctuating velocity and magnetic field dynamics and ohmic diffusion on the large vertical scale Z. Thus, ohmic dissipation dominates viscous dissipation on the large scales since, at this order of approximation, viscous diffusion is not present in (2.72)–(2.73). This feature is consistent with the $Pm \ll 1$ limit considered here. Moreover, the QGDM is characterized by a horizontal magnetic field that is $O(Rm^{-1})$ stronger than the vertical magnetic field.

Equations (2.78)–(2.80) are a magnetic version of the quasi-geostrophic convection equations originally developed by Julien *et al.* (1998). An important feature of (2.78)–(2.79) is that both advection and diffusion only occur over the small horizontal scales (x, y) due to the anisotropic spatial structure of low Rossby number convection. The fluctuating vorticity equation (2.78) contains time-dependence, advection on the small-scales, vortex stretching is represented by the third term on the left-hand side, with the remaining terms on the right-hand side being the Lorentz force and viscous diffusion, respectively. The fluctuating momentum equation is given by (2.79) and, like the fluctuating vorticity equation, contains time-dependence and horizontal advection. The vertical pressure gradient is given by the third term on the left-hand side of (2.79), with the fluctuating geostrophic stream function ψ_0' acting as pressure since the flow is geostrophically balanced; the remaining terms on the right-hand side are the buoyancy force, the Lorentz force and viscous diffusion. The fluctuating heat equation (2.80) is also characterized by time-dependence and horizontal advection and diffusion, with the third term on the left-hand side representing advection of the mean heat by the fluctuating vertical velocity over the large-scale Z.

The fluctuating induction equation (2.81) is identical to the equation given in S74, where he noted that the fluctuating magnetic field is induced by stretching the mean magnetic field with the small-scale strain $\boldsymbol{\nabla}_\perp \boldsymbol{u}_0'$ (consistent with our low Rm approximation). The absence of the time derivative shows that the fluctuating magnetic field adjusts instantaneously relative to the fluctuating convection, showing that magnetic diffusion is much more rapid than momentum diffusion on the small-scales; this effect is consistent with a small magnetic Prandtl number limit. Alfvén waves are therefore damped out on the small horizontal scales. As with the fluctuating vorticity, momentum and heat equations, only horizontal diffusion is present in the fluctuating induction owing to spatial anisotropy. Taken with (2.78)–(2.80), we see that both viscous dissipation and ohmic dissipation are important features for the small-scale dynamics. The small-scale induction equation also shows that both the present model and the CSDM require the presence of a non-trivial mean magnetic field for the development of a dynamo; this shows that the resulting dynamo is therefore large-scale and typical of low Rm dynamos (Moffatt 1978).

Parameter	Present work	Soward	Fautrelle & Childress
Eu	ϵ^{-2}	ϵ^{-2}	ϵ^{-2}
Re	$O(1)$	$\epsilon^{1/2}$	$\epsilon^{1/2}$
M	$\epsilon^{-1/2}$, $O(1)$	$\epsilon^{3/2}$	$\epsilon^{1/2}$
Γ	$\widetilde{\Gamma}\epsilon^{-1}$	$\widetilde{\Gamma}\epsilon^{-1}$	$\widetilde{\Gamma}\epsilon^{-1}$
Pe	$O(1)$	$\epsilon^{1/2}$	$\epsilon^{1/2}$
Rm	$\epsilon^{1/2}$, $O(1)$	$\epsilon^{1/2}$	$\epsilon^{1/2}$
Pr	$O(1)$	$O(1)$	$O(1)$
Pm	$\epsilon^{1/2}$, $O(1)$	$O(1)$	$O(1)$
A_X	$\epsilon^{-3/2}$	—	—
A_Z	ϵ^{-1}	ϵ^{-1}	ϵ^{-1}
A_τ	$\epsilon^{-3/2}$	$\epsilon^{-3/2}$	$\epsilon^{-3/2}$
A_T	ϵ^{-2}	—	—

TABLE 1. Comparison between the different distinguished limits taken in the present work and those of Soward (1974) and Fautrelle & Childress (1982), relative to (2.22)–(2.29*a*,*b*). We note that both Soward and Fautrelle & Childress considered weakly nonlinear motions and only a single (slow) time scale and a single large-scale coordinate in the governing equations such that $\partial_t = \partial_T = \partial_X = \partial_Y \equiv 0$. In all models the small parameter is the Rossby number, $Ro = \epsilon$, and the reduced buoyancy number $\widetilde{\Gamma} = O(1)$.

3.2. *The $Rm = O(1)$ limit*

The $Rm = O(1)$ case is associated with an order one magnetic Prandtl number. For this reason, the $Pm = O(1)$ QGDM may be particularly important for relating to DNS studies where reducing Pm to physically realistic values is impossible given the modest Reynolds numbers attainable with current computational resources. Given that, apart from the Lorentz force, the momentum and energy equations are identical to the low Pm QGDM discussed in the previous section, we focus here on the differences associated with the form of the induction equations (2.87)–(2.89).

The distinguished limit $A_\tau = \epsilon^{-1}$ shows that, in comparison to the $Rm = O(\epsilon^{1/2})$ case, the mean magnetic field now evolves on a faster time scale. The $M = O(1)$ limit indicates that the magnetic and kinetic energies are now equipartitioned when $Pm = O(1)$ – a result that appears to be consistent with DNS investigations (Stellmach & Hansen 2004).

The absence of Z-derivatives in (2.87)–(2.88) shows that ohmic dissipation is weak on the large-scales and limited to magnetic boundary layers adjacent to the horizontal boundaries. The small-scale induction equation (2.89) contains time-dependence, advection by the fluctuating velocity field, along with stretching and diffusion. The presence of $\partial_t \langle \boldsymbol{b}_0' \rangle$ results in a fluctuating magnetic field that no longer adjusts instantaneously to the fluctuating velocity field as it does when $Pm \ll 1$. For this case, Alfvén waves are present on the small fluctuating scales.

3.3. *Relationship with the Childress–Soward dynamo model (CSDM)*

In table 1 we list the different distinguished limits employed in the present work and those used by S74 and FC82. Although we have considered two limits of Rm

that result in different limits of M, Pm, and A_τ, the present discussion will be focused on the $Rm = O(\epsilon^{1/2})$ (low Pm) QGDM. Both the weak and intermediate field forms of the CSDM can be derived directly from (2.22)–(2.29) by employing the distinguished limits listed under the columns labelled 'Soward' and 'Fautrelle & Childress', respectively, and taking $\partial_t = \partial_T = \partial_X = \partial_Y \equiv 0$. The consequence of taking $Re = Pe = O(\epsilon^{1/2})$ is that the resulting models are weakly nonlinear since (horizontal) viscous diffusion enters at higher order than the advective nonlinearities in the fluctuating momentum equation. While in the present work we have considered both low and order one Pm, the CSDM employs $Pm = O(1)$. Additionally, the magnetic field scaling $M^S = \epsilon^{3/2}$ employed by S74 and $M^{FC} = \epsilon^{1/2}$ employed by FC82 contrasts sharply with our $M = \epsilon^{-1/2}$ limit; the result is that magnetic energy is significantly larger than the kinetic energy in the present work.

CS72 described three different classes of dynamos, distinguished by the relative strength of the magnetic field. In their work, the classification was based on the magnitude of the large-scale Hartmann number defined as

$$Ha_H = \frac{\mathscr{B}H}{(\mu\rho\nu\eta)^{1/2}}. \tag{3.1}$$

In the CS72 terminology, the weak field, intermediate field and strong field dynamos are characterized by Hartmann numbers of magnitude $Ha_H^w = O(1)$, $Ha_H^i = O(\epsilon^{-1/2})$ and $Ha_H^s \gg \epsilon^{-1/2}$, respectively. FC82 more precisely identified the strong field regime by the scaling $Ha_H^s = \epsilon^{-3/2}$ since this results in a Lorentz force that is comparable in strength to the Coriolis force. By employing our distinguished limits, the large-scale Hartmann number in the present work is given by

$$Ha_H^* = \frac{(MRm)^{1/2}}{\epsilon} = \frac{1}{\epsilon}. \tag{3.2}$$

Thus, by the classifications of CS72 and FC82 the present model considers magnetic fields with strengths that lie between the intermediate and strong field limits. As the fluctuating momentum equation (2.69) shows, both the Lorentz force and horizontal viscous diffusion enter the prognostic equation at the same order in our model; the result is that the small-scale Hartmann number is unity, $Ha^* = 1$.

A strong field dynamo is synonymous with the magnetostrophic balance, whereby the Coriolis, pressure gradient and Lorentz forces are of comparable magnitude. Our present model is geostrophically balanced on both the large and small scales, though as (2.51) shows a magnetostrophic balance does appear at higher, but subdominant, order in the mean momentum equation. A commonly employed dimensionless measure of the strong field dynamo is the Elsasser number, defined as the ratio of the Lorentz force to the Coriolos force and often expressed as

$$\Lambda = \frac{\mathscr{B}^2}{2\Omega\rho\mu\eta}. \tag{3.3}$$

In terms of the non-dimensional parameters and distinguished limits employed in the present study (e.g. table 1) we have

$$\Lambda^* = MPmRoRe = \epsilon. \tag{3.4}$$

Thus, as expected, the Elsasser number is small in our geostrophically balanced model. The above scaling is also consistent with previous quasi-geostrophic magnetocon-

vection studies (cf. Jones, Mussa & Worland 2003; Gillet *et al.* 2007). In S74 and FC82 the Elsasser number is significantly smaller with $\Lambda^S = \epsilon^3$ and $\Lambda^{FC} = \epsilon^2$, respectively. Although DNS studies are often characterized by order one Elsasser number, we note that these models are all limited to $Pm \sim O(1)$ and moderate values of the Ekman number. We speculate that if these models could increase their magnetic Reynolds number solely by increasing their Reynolds number and decreasing the Ekman number, rather than increasing Pm, they would begin to reach significantly smaller Elsasser numbers; this trend may be apparent in the plane layer DNS investigation of Stellmach & Hansen (2004) and the spherical DNS study of Christensen & Aubert (2006). Also, we note that the value of the Elsasser number is also dependent upon how one scales the magnetic field. The form given by (3.3) is dependent upon the magnetic diffusivity, and independent of the velocity and length scales that are important for assessing dynamical balances; this is because it is typically assumed that the magnitude of the current density scales as $\mathscr{J} \sim U\mathscr{B}/\mu\eta$ (e.g. Davidson 2001). To be consistent, the Elsasser number should be defined directly from the governing equations as

$$\widetilde{\Lambda} = \frac{\dfrac{1}{\rho\mu}\boldsymbol{B}\cdot\boldsymbol{\nabla}\boldsymbol{B}}{2\Omega\widehat{\boldsymbol{z}}\times\boldsymbol{u}} = \frac{\mathscr{B}^2}{2\Omega\,\rho\mu l\mathscr{U}}. \tag{3.5}$$

In the present work we have

$$\widetilde{\Lambda}^* = MRo = \epsilon^{1/2}. \tag{3.6}$$

Similarly, for the $Rm = O(1)$ QGDM, this gives $\widetilde{\Lambda}^* = \epsilon$. This shows that although the Elsasser number is still small, it is independent of the magnetic diffusivity. Given that the model developed in the present work is characterized by small Elsasser number, yet the magnetic energy is asymptotically larger than the kinetic energy for the low Pm QGDM, we can generally say that the partitioning of magnetic and kinetic energy is not necessarily indicative of dominant balances present within the governing equations.

Finally, we note that it is possible to extend the CSDM to include fully nonlinear motions, a strong magnetic field, and small Pm by neglecting the large-scale horizontal modulations (i.e. $\partial_X = \partial_Y = 0$) appearing in (2.73)–(2.82); the result is given by

$$\partial_Z\overline{\Psi}_{1/2} = \frac{\widetilde{Ra}}{Pr}\overline{\theta}_0, \tag{3.7}$$

$$\partial_T\overline{\theta}_0 + \partial_Z\overline{\left(w_0'\theta_1'\right)} = \frac{1}{Pr}\partial_Z^2\overline{\theta}_0, \tag{3.8}$$

$$\partial_\tau\overline{\boldsymbol{B}}_0^{\perp} = \widehat{\boldsymbol{z}}\times\partial_Z\overline{\left(\boldsymbol{u}_0'\times\langle\boldsymbol{b}_{1/2}'\rangle\right)} + \frac{1}{\widetilde{Pm}}\partial_Z^2\overline{\boldsymbol{B}}_0^{\perp}, \tag{3.9}$$

$$\partial_t\nabla_\perp^2\psi_0' + \mathrm{J}(\psi_0', \nabla_\perp^2\psi_0') - \partial_Z w_0' = \widehat{\boldsymbol{z}}\cdot\boldsymbol{\nabla}\times\left(\overline{\boldsymbol{B}}_0\cdot\boldsymbol{\nabla}_\perp\langle\boldsymbol{b}_{1/2}'\rangle\right) + \nabla_\perp^4\psi_0', \tag{3.10}$$

$$\partial_t w_0' + \mathrm{J}(\psi_0', w_0') + \partial_Z\psi_0' = \frac{\widetilde{Ra}}{Pr}\langle\theta_1'\rangle + \overline{\boldsymbol{B}}_0\cdot\boldsymbol{\nabla}_\perp\langle b_{1/2}'^{(z)}\rangle + \nabla_\perp^2 w_0', \tag{3.11}$$

$$\partial_t\langle\theta_1'\rangle + \mathrm{J}(\psi_0', \langle\theta_1'\rangle) + w_0'\partial_Z\overline{\theta}_0 = \frac{1}{Pr}\nabla_\perp^2\langle\theta_1'\rangle, \tag{3.12}$$

$$0 = \overline{\boldsymbol{B}}_0^{\perp}\cdot\boldsymbol{\nabla}_\perp\boldsymbol{u}_0' + \frac{1}{\widetilde{Pm}}\nabla_\perp^2\langle\boldsymbol{b}_{1/2}'\rangle \tag{3.13}$$

and we note that the solenoidal conditions given by (2.77) and (2.82) are identically satisfied.

3.4. *Applications to natural dynamos*

It is informative to compare the distinguished limits that were taken in the present work with what is known about the geodynamo and other natural dynamos; this exercise is useful for establishing the strengths and weaknesses of the present model. Three time scales are necessary to allow time variations of the fluctuating convection, the mean magnetic field and the mean temperature. To observe an order one change in the mean magnetic field, for instance, requires convective time scales of $t = O(\epsilon^{-3/2})$. Similarly, convective time scales of $t = O(\epsilon^{-2})$ are required to observe order one changes in the mean temperature time scale. This implies the relative ordering of these time scales is given by

$$t \ll t_B \ll t_\theta, \tag{3.14}$$

where t_B and t_θ are the mean magnetic and temperature evolution time scales measured in the units of the convective time scale t. This ordering states that the large-scale magnetic evolution time scale lies midway between the small-scale convective time scale and the large-scale thermal evolution time scale. For the geodynamo, observations of the geomagnetic field show that $t \sim O(10^2)$ years, $t_B \sim O(10^4)$ years and $t_\theta \sim O(10^9)$ years, suggesting that the above ordering is realistic.

Utilizing the velocity based on the small-scale viscous diffusion time scale, the (small-scale) Rossby number can be related to the large-scale Ekman number as

$$\epsilon = Ro = Ek^{1/3}. \tag{3.15}$$

Studies suggest that the viscosity of the Earth's core is similar to that of water at standard temperature and pressure (e.g. Pozzo *et al.* 2013) such that $Ek \sim O(10^{-15})$ where the depth of the core $H \approx 2265$ km. Estimates for the small-scale Rossby number, and the large-scale magnetic and hydrodynamic Reynolds numbers are given by, respectively,

$$\epsilon = 10^{-5}, \tag{3.16}$$

$$Rm_H = RmEk^{-1/3} = \epsilon^{-1/2} \sim O(10^2), \tag{3.17}$$

$$Re_H = ReEk^{-1/3} = 10^5 Re. \tag{3.18}$$

Observations find typical flow speeds in the core to be $U \approx 4 \times 10^{-4}$ m s^{-1} (Finlay & Amit 2011); whether this characteristic speed corresponds to the small- or large-scale flows is unknown. If the convective velocities are significantly larger than the mean flows in the core, as in the asymptotic model presented here, then it is possible these speeds may be associated with the small-scale convection. Estimating a typical convective scale in the core as $\ell_{core} \sim HEk^{1/3} \approx 30$ m, an estimate for the small-scale Rossby number in the core is $Ro_{core} \approx 0.1$. Although this estimate is larger than our above estimate from the asymptotic scalings, it is less than unity such that quasi-geostrophic theory may be an accurate description of the dynamics (e.g. Pedlosky 1987; Stellmach *et al.* 2014). The large-scale magnetic Reynolds number estimate given above possesses the correct order of magnitude estimate for the core. For the large-scale Reynolds number Re_H we require knowledge of the small-scale Reynolds number Re; estimating this value leads to $Re_{core} \approx 1200$. The large-scale Reynolds number estimate for the core is then $Re_H \sim O(10^9)$; a number that is in agreement with observations and suggests that the QGDM may be in the appropriate dynamical regime necessary for understanding the geodynamo.

The current model assumes an order one small-scale Reynolds number; coupled with the relationship $Rm = RePm$, this implies that $Pm = O(\epsilon^{1/2})$. The magnetic Prandtl

number in the Earth's core is thought to be $Pm \sim O(10^{-6})$, so it would seem that the distinguished limit taken for Pm is not quite in line with what typical values are in the Earth's core. However, the theory developed here suggests that $Pm = O(\epsilon^{1/2})$ is sufficiently small to be in the asymptotic limit of small magnetic Prandtl number; we can then reach smaller magnetic Prandtl numbers by reducing $\widetilde{Pm}$. Furthermore, the distinguished limit of $M = O(\epsilon^{-1/2})$ shows that magnetic energy dominates when $Pm \ll 1$; this result is thought to be generally consistent with what is known about the geodynamo.

As previously mentioned, we have chosen to non-dimensionalize the equations based on those dimensional quantities that possess the maximum amplitude; this implies that some non-dimensional parameters will contain a 'mix' of large- and small-scale dimensional quantities. Because of the importance of the small-scale motions, the dimensional length and velocity scales are then the small scales l and $\mathscr{U}$, respectively. Pressure, temperature and magnetic field were then based on the large-scale mean quantities. Any dimensionless parameter can be rescaled to be only a function of the small- or large-scale dimensional quantities by noting the asymptotic relations that were employed in the present work. For instance, the magnetic to kinetic energy ratio M is based on the large-scale magnetic field and the small-scale velocity field. When expressed solely in terms of the large-scale variables we have $\overline{M} = \epsilon^{-1} M \approx 10^7$ where we've used the ϵ estimate given by (3.16).

Assuming a large-scale magnetic field strength of $O(10^{-3})$ Tesla for the core (e.g. Gillet *et al.* 2010), the traditionally defined Elsasser number (3.3) is $\Lambda = O(1)$. The model presented here is not capable of matching this value and represents one of the most significant discrepancies between the present work and what is presently known about the geodynamo. With the exception of Jupiter, however, estimates suggest that the Elsasser number for other planetary dynamos is significantly less than unity (Schubert & Soderlund 2011). As stated previously, the traditionally defined Elsasser number may not be an accurate indicator of the dominant force balance in the core as numerical simulations show that dynamos characterized by $\Lambda = O(1)$ remain geostrophically balanced (Soderlund *et al.* 2012).

We emphasize that some care must be taken with regard to estimating the dominant balance in DNS. Taking the curl of the momentum equation appears to be a common approach for determining the dominant force balance in simulations (St Pierre 1993; Christensen & Aubert 2006; King & Buffett 2013). Such a procedure can often lead to an erroneous conclusion, since the action of curling the momentum equation will automatically filter a dominant geostrophic balance. This is indeed the case for the present model where leading order geostrophic balances identified in (2.50) and (2.66) are removed by the curling operation. For instance, (2.53) shows that taking the curl of the mean momentum equation (2.50) yields the trivial result up to $O(\epsilon^{1/2})$. The first non-trivial result arises at $O(\epsilon)$ by curling the mean momentum equation (2.51) and will yield a vorticity equation involving a (vorticity) balance between the curl of the Coriolis and Lorentz force terms; this should not be interpreted as a force balance between the Coriolis and Lorentz forces (e.g. St Pierre 1993). The salient point is that dominant balances can only be determined directly from the momentum equation, and not from the vorticity equation. Rather, analysis of the terms present in the vorticity equation for a geostrophically balanced flow will tell you which forces act as small perturbations to the main geostrophic balance.

The alternative definition of the Elsasser number given by (3.5), is $O(10^{-2})$ for the geodynamo, suggesting that the Lorentz force may not enter the leading order force balance for the large-scale dynamics of the core (Nataf & Schaeffer 2015). Moreover,

previous work calculating the angular momentum of the Earth's outer core must invoke geostrophy to obtain the large-scale velocity field within the core, and shows excellent agreement with values obtained independently from observations of the Earth's rotation rate (Jault *et al.* 1988; Jackson *et al.* 1993; Gillet *et al.* 2010, 2012; Schaeffer & Pais 2011). These results suggest that a large-scale thermal wind model, similar to the one developed here, may be relevant for understanding the physics of the geodynamo. Of course, the large-scale thermal wind model is characterized by $A_X \gg A_Z$ and is therefore unlike that of a deep spherical shell where the aspect ratio is order one. We were unable to obtain a closed large-scale model with $A_X = A_Z$ that is coupled to the small-scale dynamics; future work is necessary to determine if this difficulty can be circumvented in a spherical geometry.

The present work has utilized an expansion based on the smallness of the small-scale Rossby number. As discussed by Nataf & Schaeffer (2015), the precise value of the small-scale Rossby number depends upon the detailed properties of the turbulence that is controlled by the relative importance of inertia, buoyancy and the small-scale magnetic field. Nataf & Schaeffer (2015) argue that although the Elsasser number, as given by (3.5), is $O(0.01)$ for the largest scales of the Earth's core, it may increase to $O(1–10)$ on the scale of about 10 km such that the Lorentz force becomes more significant as the length scale is reduced. Indeed, as the QGDM shows, if the Lorentz force is subdominant on the largest scales then it must be present in the small-scale dynamics for the dynamo to reach a saturated, non-kinematic state. Future numerical simulations of the QGDM should therefore help to understand the small-scale dynamics of the geodynamo and other planetary magnetic fields (e.g. Stanley & Glatzmaier 2010).

4. Conclusion

In the present work we have utilized a standard multiple scales asymptotic approach to develop a new multiscale dynamo model that is valid in the limit of small Rossby number. The small-scale model is characterized by a magnetically modified version of the quasi-geostrophic convection equations originally developed by Julien *et al.* (1998) and later studied in detail by Sprague *et al.* (2006). The large-scale model is characterized by a thermal wind balance in the mean momentum equations; coupled with the mean heat equation, the large-scale model is equivalent to the well-known planetary geostrophy equations commonly employed for investigating the dynamics of the Earth's atmosphere and ocean. We have discussed both low and order one magnetic Prandtl number models, showing that these two cases possess fundamentally different properties. For the low Pm case the magnetic energy dominates the kinetic energy, and ohmic dissipation is asymptotically dominant over viscous dissipation on the large-scales. When $Pm = O(1)$, it was demonstrated that the magnetic and kinetic energies become equipartitioned with weak large-scale ohmic dissipation. In both cases the dynamics are characterized by small Elsasser number since the motions are geostrophically balanced. The new model can be considered a fully nonlinear, generalized version of the dynamo model originally developed by Childress & Soward (1972).

Numerical simulations of asymptotically reduced equation sets have proven useful for accessing dynamical regimes in rotating plane layer convection that are computationally demanding or impossible to reach with the use of DNS (e.g. Sprague *et al.* 2006; Julien *et al.* 2012*a*,*b*; Rubio *et al.* 2014; Stellmach *et al.* 2014). These investigations have shown the dependence of the flow regime on both the Rayleigh

and Prandtl numbers, new phenomena such as an asymptotic heat transfer scaling regime (Julien *et al.* 2012*a*), and large-scale vortex formation via an inverse cascade (Julien *et al.* 2012*b*). Future simulations of the new model will help to shed light on the interaction of these phenomena with a magnetic field. For instance, a recent DNS investigation by Guervilly, Hughes & Jones (2015) has shown that large-scale vortices can play a significant role in generating large-scale magnetic fields, particularly as the magnetic Prandtl number is reduced below one.

Various extensions of the present work can also be carried out. While we have assumed, for simplicity, that the fluid is Boussinesq and that the gravity vector and rotation vector are aligned, it is a straightforward procedure to relax both of these constraints to include compressibility and varying angle between the gravity and rotation vectors (Julien *et al.* 2006; Mizerski & Tobias 2013). Although the anelastic approximation appears to agree well with the compressible equations for the case of order one Prandtl numbers (Calkins, Julien & Marti 2014), it has recently been shown that it yields spurious results for low Prandtl number quasi-geostrophic convection (Calkins, Julien & Marti 2015). However, Calkins *et al.* (2015) outlined an approach for extending the Boussinesq quasi-geostrophic convection equations of Sprague *et al.* (2006) to the case of a fully compressible gas.

The present model has focused on the plane layer geometry for the sake of mathematical and physical simplicity. To further the applicability of the present work with that of natural systems, it will be useful to extend the present methodology to the rotating cylindrical annulus (Busse 1986) and to spherical geometries. The three-dimensional cylindrical annulus model recently developed by Calkins *et al.* (2013) is particularly interesting since it possesses order one axial velocties, such that the Ekman pumping dynamo effect investigated by Busse (1975) is no longer a prerequisite for dynamo action in this geometry.

Acknowledgements

The authors thank S. Childress, three anonymous referees and M. Plumley for helpful comments that improved the manuscript greatly. This work was supported by the National Science Foundation under grants EAR no. 1320991 (M.A.C., K.J. and J.M.A.) and EAR CSEDI no. 1067944 (K.J. and J.M.A.).

REFERENCES

BENDER, C. M. & ORSZAG, S. A. 2010 *Advanced Mathematical Methods for Scientists and Engineers I: Asymptotic Methods and Perturbation Theory*. Springer.

BUSSE, F. H. 1975 A model of the geodynamo. *Geophys. J. R. Astron. Soc.* **42**, 437–459.

BUSSE, F. H. 1986 Asymptotic theory of convection in a rotating, cylindrical annulus. *J. Fluid Mech.* **173**, 545–556.

CALKINS, M. A., JULIEN, K. & MARTI, P. 2013 Three-dimensional quasi-geostrophic convection in the rotating cylindrical annulus with steeply sloping endwalls. *J. Fluid Mech.* **732**, 214–244.

CALKINS, M. A., JULIEN, K. & MARTI, P. 2014 Onset of rotating and non-rotating convection in compressible and anelastic ideal gases. *Geophys. Astrophys. Fluid Dyn.* **109** (4), 422–449.

CALKINS, M. A., JULIEN, K. & MARTI, P. 2015 The breakdown of the anelastic approximation in rotating compressible convection: implications for astrophysical systems. *Proc. R. Soc. Lond.* A **471**, 20140689.

CHANDRASEKHAR, S. 1961 *Hydrodynamic and Hydromagnetic Stability*. Oxford University Press.

CHARNEY, J. G. 1948 On the scale of atmospheric motions. *Geophys. Publ.* **17**, 3–17.

CHILDRESS, S. & SOWARD, A. M. 1972 Convection-driven hydromagnetic dynamo. *Phys. Rev. Lett.* **29** (13), 837–839.

CHINI, G., JULIEN, K. & KNOBLOCH, E. 2009 An asymptotically reduced model of turbulent Langmuir circulation. *Geophys. Astrophys. Fluid Dyn.* **103** (2–3), 179–197.

CHRISTENSEN, U. & AUBERT, J. 2006 Scaling properties of convection-driven dynamos in rotating shells and applications to planetary magnetic fields. *Geophys. J. Intl* **166**, 97–114.

DAVIDSON, P. A. 2001 *An Introduction to Magnetohydrodynamics*. Cambridge University Press.

DOLAPTCHIEV, S. I. & KLEIN, R. 2009 Planetary geostrophic equations for the atmosphere with evolution of barotropic flow. *Dyn. Atmos. Oceans* **46**, 46–61.

FAUTRELLE, Y. & CHILDRESS, S. 1982 Convective dynamos with intermediate and strong fields. *Geophys. Astrophys. Fluid Dyn.* **22** (3), 235–279.

FAVIER, B. & PROCTOR, M. R. E. 2013 Kinematic dynamo action in square and hexagonal patterns. *Phys. Rev.* E **88**, 053011.

FINLAY, C. C. & AMIT, H. 2011 On flow magnitude and field-flow alignment at Earth's core surface. *Geophys. J. Intl* **186**, 175–192.

GILLET, N., BRITO, D., JAULT, D. & NATAF, H.-C. 2007 Experimental and numerical studies of magnetoconvection in a rapidly rotating spherical shell. *J. Fluid Mech.* **580**, 123–143.

GILLET, N., JAULT, D., CANET, E. & FOURNIER, A. 2010 Fast torsional waves and strong magnetic field within the Earth's core. *Nature* **465**, 74–77.

GILLET, N., SCHAEFFER, N. & JAULT, D. 2012 Rationale and geophysical evidence for quasi-geostrophic rapid dynamics within the Earth's outer core. *Phys. Earth Planet. Inter.* **202–203**, 78–88.

GROOMS, I., JULIEN, K. & FOX-KEMPER, B. 2011 On the interactions between planetary geostrophy and mesoscale eddies. *Dyn. Atmos. Oceans* **51**, 109–136.

GUERVILLY, C., HUGHES, D. W. & JONES, C. A. 2015 Generation of magnetic fields by large-scale vortices in rotating convection. *Phys. Rev.* E **91**, 041001.

HAUT, T. & WINGATE, B. 2014 An asymptotic parallel-in-time method for highly oscillatory PDES. *SIAM J. Sci. Comput.* **36** (2), A693–A713.

JACKSON, A., BLOXHAM, J. & GUBBINS, D. 1993 Time-dependent flow at the core surface and conservation of angular momentum in the coupled core-mantle system. *Dyn. Earth's Deep Interior Earth Rotation* **72**, 97–107.

JAULT, D., GIRE, C. & MOUËL, J. L. L. 1988 Westward drift, core motions and exchanges of angular momentum between core and mantle. *Nature* **333**, 353–356.

JONES, C. A. 2011 Planetary magnetic fields and fluid dynamos. *Annu. Rev. Fluid Mech.* **43**, 583–614.

JONES, C. A., MUSSA, A. I. & WORLAND, S. J. 2003 Magnetoconvection in a rapidly rotating sphere: the weak-field case. *Proc. R. Soc. Lond.* A **459**, 773–797.

JULIEN, K. & KNOBLOCH, E. 2007 Reduced models for fluid flows with strong constraints. *J. Math. Phys.* **48**, 065405.

JULIEN, K., KNOBLOCH, E., MILLIFF, R. & WERNE, J. 2006 Generalized quasi-geostrophy for spatially anistropic rotationally constrained flows. *J. Fluid Mech.* **555**, 233–274.

JULIEN, K., KNOBLOCH, E., RUBIO, A. M. & VASIL, G. M. 2012*a* Heat transport in Low-Rossby-number Rayleigh–Bénard Convection. *Phys. Rev. Lett.* **109**, 254503.

JULIEN, K., KNOBLOCH, E. & WERNE, J. 1998 A new class of equations for rotationally constrained flows. *Theor. Comput. Fluid Dyn.* **11**, 251–261.

JULIEN, K., RUBIO, A. M., GROOMS, I. & KNOBLOCH, E. 2012*b* Statistical and physical balances in low Rossby number Rayleigh–Bénard convection. *Geophys. Astrophys. Fluid Dyn.* **106** (4-5), 392–428.

KING, E. M. & BUFFETT, B. A. 2013 Flow speeds and length scales in geodynamo models: the role of viscosity. *Earth Planet. Sci. Lett.* **371**, 156–162.

KLEIN, R. 2010 Scale-dependent models for atmospheric flows. *Annu. Rev. Fluid Mech.* **42**, 249–274.

MALECHA, Z., CHINI, G. & JULIEN, K. 2014 A multiscale algorithm for simulating spatially-extended Langmuir circulation dynamics. *J. Comput. Phys.* **271**, 131–150.

MIESCH, M. S. 2005 Large-scale dynamics of the convection zone and tachocline. *Living Rev. Solar Phys.* **2** (1), available online at http://solarphysics.livingreviews.org/Articles/lrsp-2005-1/.

MIZERSKI, K. A. & TOBIAS, S. M. 2013 Large-scale convective dynamos in a stratified rotating plane layer. *Geophys. Astrophys. Fluid Dyn.* **107** (1-2), 218–243.

MOFFATT, H. K. 1978 *Magnetic Field Generation in Electrically Conducting Fluids*. Cambridge University Press.

MOFFATT, H. K. 2008 Magnetostrophic turbulence and the geodynamo. In *IUTAM Symposium on Computational Physics and New Perspectives in Turbulence*, pp. 339–346. Springer.

NATAF, H.-C. & SCHAEFFER, N. 2015 Turbulence in the core. In *Treatise on Geophysics* (ed. P. Olson & G. Schubert), vol. 8. Elsevier.

PARKER, E. N. 1955 Hydromagnetic dynamo models. *Astrophys. J.* **122**, 293–314.

PEDLOSKY, J. 1987 *Geophysical Fluid Dynamics*. Springer.

PHILLIPS, N. A. 1963 Geostrophic motion. *Rev. Geophys.* **1** (2), 123–176.

POZZO, M., DAVIES, C. J., GUBBINS, D. & ALFÉ, D. 2013 Transport properties for liquid silicon–oxygen–iron mixtures at Earth's core conditions. *Phys. Rev.* B **87**, 014110.

ROBERTS, P. H. 1988 Future of geodynamo theory. *Geophys. Astrophys. Fluid Dyn.* **44**, 3–31.

ROBINSON, A. & STOMMEL, H. 1959 The oceanic thermocline and the associated thermohaline circulation. *Tellus* **11**, 295–308.

ROTVIG, J. & JONES, C. A. 2002 Rotating convection-driven dynamos at low Ekman number. *Phys. Rev.* E **66**, 056308.

RUBIO, A. M., JULIEN, K., KNOBLOCH, E. & WEISS, J. B. 2014 Upscale energy transfer in three-dimensional rapidly rotating turbulent convection. *Phys. Rev. Lett.* **112**, 144501.

SCHAEFFER, N. & PAIS, M. A. 2011 On symmetry and anisotropy of Earth-core flows. *Geophys. Res. Lett.* **38**, L10309.

SCHUBERT, G. & SODERLUND, K. 2011 Planetary magnetic fields: observations and models. *Phys. Earth Planet. Inter.* **187**, 92–108.

SODERLUND, K. M., KING, E. M. & AURNOU, J. M. 2012 The influence of magnetic fields in planetary dynamo models. *Earth Planet. Sci. Lett.* **333–334**, 9–20.

SOWARD, A. M. 1974 A convection-drive dynamo. Part I: the weak field case. *Phil. Trans. R. Soc. Lond.* A **275**, 611–646.

SPRAGUE, M., JULIEN, K., KNOBLOCH, E. & WERNE, J. 2006 Numerical simulation of an asymptotically reduced system for rotationally constrained convection. *J. Fluid Mech.* **551**, 141–174.

ST PIERRE, M. G. 1993 The strong field branch of the Childress–Soward dynamo. In *Theory of Solar and Planetary Dynamos* (ed. M. R. E. Proctor, P. C. Matthews & A. M. Rucklidge), pp. 295–302. Cambridge University Press.

STANLEY, S. & GLATZMAIER, G. A. 2010 Dynamo models for planets other than Earth. *Space Sci. Rev.* **152**, 617–649.

STEENBECK, M. & KRAUSE, F. 1966 The generation of stellar and planetary magnetic fields by turbulent dynamo action. *Z. Naturforsch.* a **21**, 1285–1296.

STEENBECK, M., KRAUSE, F. & RÄDLER, K.-H. 1966 A calculation of the mean electromotive force in an electrically conducting fluid in turbulent motion, under the influence of coriolis forces. *Z. Naturforsch.* a **21**, 369–376.

STELLMACH, S. & HANSEN, U. 2004 Cartesian convection driven dynamos at low Ekman number. *Phys. Rev.* E **70**, 056312.

STELLMACH, S., LISCHPER, M., JULIEN, K., VASIL, G., CHENG, J. S., RIBEIRO, A., KING, E. M. & AURNOU, J. M. 2014 Approaching the asymptotic regime of rapidly rotating convection: boundary layers versus interior dynamics. *Phys. Rev. Lett.* **113**, 254501.

STEWARTSON, K. & CHENG, H. K. 1979 On the structure of inertial waves produced by an obstacle in a deep, rotating container. *J. Fluid Mech.* **91**, 415–432.

WEINAN, E., ENGQUIST, B., LI, X., REN, W. & VANDEN-EIJNDEN, E. 2007 Heterogeneous multiscale methods: a review. *Commun. Comput. Phys.* **2** (3), 367–450.

WELANDER, P. 1959 An advective model for the ocean thermocline. *Tellus* **11**, 309–318.